Auger decay of the 3*d* hole in the isoelectronic series of Br, Kr^+, and Rb^{2+}

J. Keskinen,[1,*] K. Jänkälä,[1] S.-M. Huttula,[1] T. Kaneyasu,[2] Y. Hikosaka,[3] E. Shigemasa,[4] H. Iwayama,[4] K. Soejima,[5] K. Ito,[6] L. Andric,[7] M. A. Khalal,[7] J. Palaudoux,[7] F. Penent,[7] and P. Lablanquie[7]

[1]*Nano and Molecular Systems Research Unit, University of Oulu, P.O. Box 3000, 90014 Oulu, Finland*
[2]*SAGA Light Source, Tosu 841-0005, Japan*
[3]*Institute of Liberal Arts and Sciences, University of Toyama, Toyama 930-0194, Japan*
[4]*Institute for Molecular Science, Okazaki 444-8585, Japan*
[5]*Department of Environmental Science, Niigata University, Niigata 950-2181, Japan*
[6]*Société Civile Synchrotron SOLEIL, L'Orme des Merisiers, Saint-Aubin, Boîte Postale 48, 91192 Gif-sur-Yvette Cedex, France*
[7]*Sorbonne Université, CNRS, Laboratoire de Chimie Physique-Matière et Rayonnement, 4 Place Jussieu, 75005 Paris, France*

(Received 30 September 2020; accepted 11 February 2021; published 22 March 2021)

The Auger decay process of the $3d_{5/2}$ hole is studied experimentally and theoretically along the isoelectronic Br, Kr^+, and Rb^{2+} series with electron configuration [Ar] $3d^9 4s^2 4p^6$. The experimental results consist of multielectron coincidence data measured from all three elements and conventional high-resolution Auger spectrum for the Br case. Theoretical interpretation was done by using multiconfiguration Dirac-Fock calculations. It is found that the decay rate of two-Auger-electron emission increases along the series in the direction of decreasing nuclear charge. Also, complexity of the Auger spectrum follows the same trend, requiring a drastic increase to the size of the configuration space for describing the observed spectra.

DOI: 10.1103/PhysRevA.103.032828

I. INTRODUCTION

Shallow inner-shell atomic holes are excited states that decay predominantly by release of a so-called "Auger electron" [1,2]. However, a weaker, "double-Auger" decay path, in which two Auger electrons are emitted, was discovered at the end of the 60s in Ne and Ar atoms [3,4]. The improvement of electron coincidence experiments brought deeper insight into this process, enabling the detailed study of the ways the double-Auger decay can proceed: through a series of decays called cascade Auger decays or through a direct process [5–8]. This direct double-Auger decay, in which the two Auger electrons are simultaneously emitted, has a lower probability but is a direct manifestation of a three-electron correlation process. Its detailed study took more time, for both experiments [6] and theory, which refers to knock-out and shake-off mechanisms [9,10]. More recently experimental evidence for a direct triple-Auger decay has also been found in C^+ ions [11] and Ar atoms [12].

In this work, we have studied the Auger decay of the 3*d* holes in the isoelectronic configuration [Ar] $3d^9 4s^2 4p^6$ in the cases of Br, Kr^+, and Rb^{2+}. We present here only the decay of the $3d_{5/2}$ component, as the two $3d_j$ spin-orbit components ($j = 3/2$ or $5/2$) behave in a similar way. The main decay of a $3d_j$ hole happens through an $M_{4,5}NN$ Auger path which has been studied extensively in Kr^+ over the time of five decades [8,13–17]. These studies have, among other things, shown that the decays of the $3d_j$ hole can proceed through a cascade Auger decay with a ∼29% probability [8]. A question arises whether a similar behavior follows the $3d_j$ hole decay in an isoelectronic Br atom and in a Rb^{2+} ion. More precisely, the question is to study the influence of the change in core charge, increasing from Br to Kr^+ and to Rb^{2+}, on the Auger decay. To the best of our knowledge, no information is available in the literature for the Rb^{2+} $3d^9 4s^2 4p^6$ system, except for a Ph.D. thesis [18]. As for the Br atom, the 3*d* photoabsorption was investigated in Refs. [19,20] and the decay of the ($3d \rightarrow 4p$) resonance was studied theoretically and experimentally by photoelectron spectroscopy [21], suggesting a dominant decay into singly ionized Br^+ states. However, no detailed information of the Auger decay pathways has been available.

As bromine is highly reactive in atomic form, the Br $3d^{-1} 4s^2 4p^6$ states are created via ultrafast dissociation of the HBr molecule upon HBr ($3d_{5/2} \rightarrow \sigma^*$) photoexcitation [22]. The observed process can be described as

$$h\nu + \mathrm{HBr} \rightarrow \mathrm{HBr}(3d \rightarrow \sigma^*) \rightarrow \mathrm{H} + \mathrm{Br}(3d^{-1}4p^6).$$

Note that the ultrafast dissociation of the HBr ($3d \rightarrow \sigma^*$) resonance is the dominant process, and it occurs in competition with the weaker autoionization paths within the HBr molecule (see Ref. [23] and the references therein for details).

The single- and double-Auger decays of 3*d* holes have been measured by electron spectroscopy after 3*d* excitation or ionization using synchrotron radiation and interpreted with theoretical predictions obtained from multiconfiguration Dirac-Fock calculations.

II. EXPERIMENT

The study used two experimental setups: the first was a multielectron coincidence spectrometer, the magnetic bottle

*juho.keskinen@oulu.fi

electron time-of-flight spectrometer HERMES [8,12]. It provides an energy resolution $\Delta E/E$ of $\sim$1.6%, where E is the kinetic energy of the electron. The second was a high-resolution hemispherical electron energy analyzer (MBS-A1) [23]. Its resolution was ΔE 20 meV, including the contribution of the analyzer (12 meV) and of the Doppler broadening (10 meV). The axis of the electrostatic lens of the analyzer was perpendicular to the photon beam and fixed at the magic angle (54.7°) relative to the direction of polarization of the incident synchrotron radiation.

The experiments on Kr and Rb were performed at the undulator beamline PLEIADES [24] of the SOLEIL synchrotron facility during the single-bunch operating mode of the synchrotron, providing bunches of light every 1184 ns. The Auger decay of the Kr^+ $3d_{5/2}^{-1}4s^24p^6$ states were obtained by analyzing coincidences with a $3d_{5/2}$ photoelectron, in a similar way as was done by Palaudoux *et al.* [8]. The Auger decay of the Rb^{2+} $3d_{5/2}^{-1}4s^24p^6$ states involved a more complex analysis, in which the Auger electrons were identified by their detection in coincidence with the pair of $3d$ and $5s$ photoelectrons. Such a procedure was previously developed to study the Auger decay of the Ar^{2+} $2p^{-1}3s^23p^5$ states [25] and applied to the study of the decay of the $4d$ hole in the Xe^+ ion [18,26].

The excited Br $3d_{5/2}^{-1}4s^24p^6$ state was created through ultrafast dissociation of the HBr molecule upon $(3d \rightarrow \sigma^*)$ excitation [22]. Its Auger decay was obtained using the multielectron coincidence setup HERMES at the undulator beamline U56/2 PGM2 [27] of the BESSY-II synchrotron radiation facility in Berlin, Germany. The synchrotron was used in single-bunch operation mode, providing bunches of light every 800.5 ns. Figure 1 displays the Auger spectra measured at the HBr $(3d_{5/2} \rightarrow \sigma^*)$ resonance. The raw spectra contain the contribution of the multiple ionization of the HBr molecule. The Auger decay of the atomic Br $3d_{5/2}^{-1}4s^24p^6$ state is obtained by subtracting an off-resonance spectrum. This is illustrated in Fig. 1(a), in which the on- and off-resonance, total one-dimensional Auger spectra are shown. The difference gives the contribution of the Br atomic Auger decay and is displayed in Fig. 1(b). It compares well with the Auger spectrum obtained with the same method by Morin and Nenner [22] and the one obtained directly on Br atoms, obtained by laser dissociation of the Br^2 molecule by Nahon *et al.* [21]. In a similar way the raw two-dimensional energy correlation map of electron-electron coincidences measured at the HBr $(3d_{5/2} \rightarrow \sigma^*)$ resonance is displayed in Fig. 1(c). Integration along the diagonal lines gives the final dicationic states shown in Fig. 1(e). The contribution associated with the double ionization of the HBr molecule is estimated off-resonance. Its subtraction gives in Fig. 1(d) the population of the Br^{2+} states populated upon double-Auger decay of the Br $3d_{5/2}^{-1}4s^24p^6$ state.

Finally a high-resolution conventional Auger spectrum of the Br $3d_{5/2}^{-1}4s^24p^6$ state was obtained with the MBS-A1 analyzer at the soft x-ray beamline BL6U at the UVSOR facility at the Institute for Molecular Science in Okazaki, Japan [23]. It is presented in Fig. 2(b). As in the previous experiment, it was obtained using the ultrafast dissociation of the HBr molecule upon $(3d_{5/2} \rightarrow \sigma^*)$ excitation. The same procedure as in Fig. 1(a) is used in Fig. 2(a) in order to extract the atomic contribution shown in Fig. 2(b). It compares well

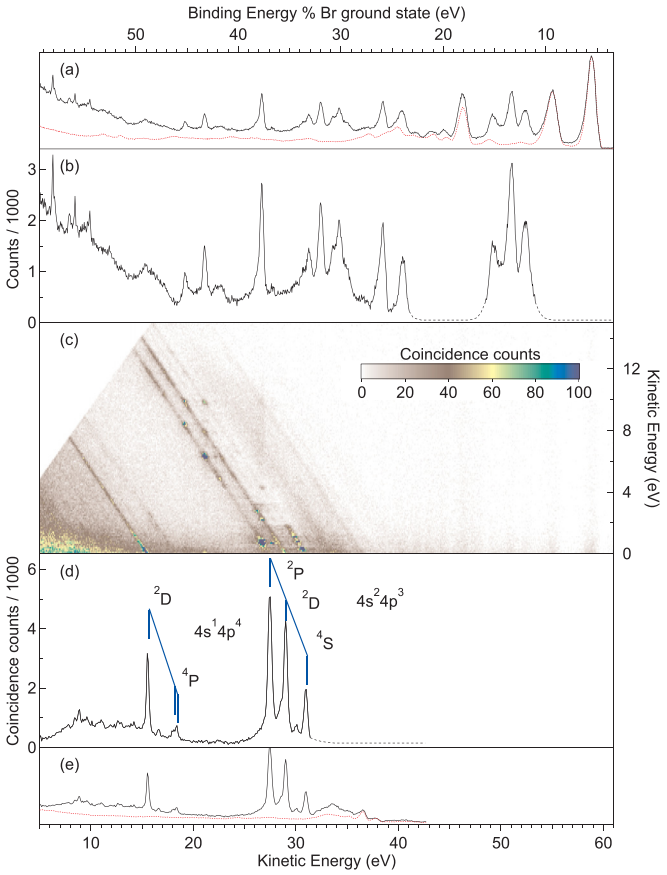

FIG. 1. (a) The electron spectrum measured on the HBr $(3d_{5/2} \rightarrow \sigma^*)$ resonance at a photon energy of $h\nu = 70.7$ eV (solid black line). It contains atomic lines due to the Auger decay of the Br atom formed upon ultrafast dissociation [22] and molecular lines due to photoionization processes in the HBr molecule. This last contribution is estimated off-resonance at 75.3 eV (dotted red line). Its subtraction gives in panel (b) the estimated Auger spectrum associated with the decay of the Br $3d_{5/2}^{-1}4s^24p^6$ state. Panel (c) represents the electron-electron energy correlation map measured on the $(3d_{5/2} \rightarrow \sigma^*)$ resonance in HBr. The recorded coincidence counts are coded by colors. Panel (e) shows the double-photoionization spectrum (solid black line) measured on the HBr $(3d_{5/2} \rightarrow \sigma^*)$ resonance, extracted by integrating diagonally the coincidence map (c), as well as the off-resonance spectrum (dotted red line). Subtraction of this molecular component gives in panel (d) the Br^{2+} dicationic states populated by double-Auger decay of the $3d_{5/2}^{-1}4s^24p^6$ state as a solid black line (the dashed part is a guide to the eye to highlight the atomic lines; the broad band above 32 eV appearing in panel (e) is due to the weaker molecular decays of the HBr $(3d \rightarrow \sigma^*)$ resonance). Each label denotes the main contributing configuration of the corresponding line group. The spectra are presented as a function of the kinetic energy of the electrons (bottom axis) or as a function of binding energy of the Br^+ and Br^{2+} states (top axis) referenced to the Br $4s^24p^5$ ($^2P_{3/2}$) ground-state level.

with the lower-resolution Auger spectra obtained previously [Fig. 1(b) or 2(c)]. The spectrum has been calibrated in energy by adopting the method used in Ref. [23], which places the $4s4p^5$ ^1P Auger line at 38.42 eV. Note that weak shadow peaks [marked with asterisks in Fig. 2(b)] are observed at a higher kinetic energy above the main Auger peaks; they are assigned

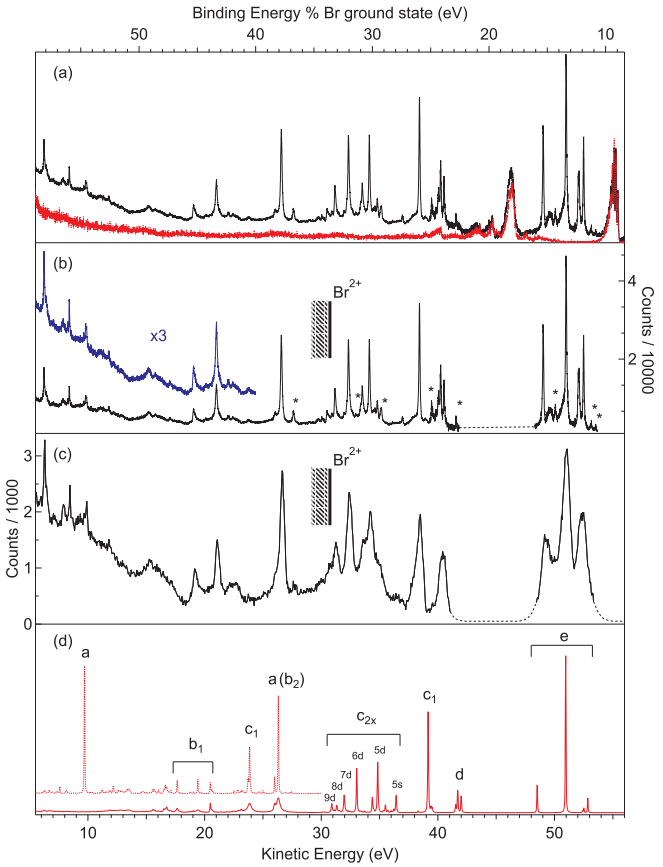

FIG. 2. Measured (b, c) and simulated (d) Auger spectra resulting from the decay of the Br $3d_{5/2}^{-1}4s^24p^6$ state. The high-resolution Auger spectrum in panel (b) has been obtained with the procedure explained for Fig. 1(a) by subtracting an off-resonance spectrum [dotted red line in panel (a)] from the spectrum measured on the HBr ($3d_{5/2} \rightarrow \sigma^*$) resonance [solid black line in panel (a)]. Panel (c) is the low-energy resolution Auger spectrum of Fig. 1(b). The dashed lines act as guides to the eye. The dotted line in panel (d) represents simulated spectra (FAC) without accounting for the line broadening due to the subsequent decay. Vertical lines with hatched areas indicate the upper kinetic energy limit for the double-Auger path. Labels correspond to the different contributing configurations in the following manner: **a**: $4s^04p^6$, $\mathbf{b_1}$: $4s4p^4(5s, 6/7/9d)$, $\mathbf{b_2}$: $4s4p^44d$, $\mathbf{c_1}$: $4s^24p^34d$, $\mathbf{c_{2x}}$: $4s^24p^3(5s, nd)$, **d**: $4s4p^5$, and **e**: $4s^24p^4$. Bracketed labels correspond to configurations that strongly mix with the main contributing configurations. In the case of $\mathbf{c_{2x}}$ additional $n/n\ell$ labeling marked above the corresponding peaks defines the configuration in more detail.

to the other spin-orbit component, that is, to the decay of the Br $3d_{3/2}^{-1}4s^24p^6$ state, because the ($3d_{3/2} \rightarrow \sigma^*$) resonance can be weakly excited at the photon energy of 70.7 eV, on top of the HBr ($3d_{5/2} \rightarrow \sigma^*$) resonance. These spurious peaks appear at about 1.04 eV above the main Auger peak, a value in agreement with the Br 3*d* spin-orbit splitting measured by Nahon *et al.* [21].

III. CALCULATIONS

Theoretical simulations were carried out using the multiconfiguration Dirac-Fock (MCDF) method with the Flexible Atomic Code (FAC) [28] and GRASP2K [29,30] to acquire predictions for the Auger decays in the studied isoelectronic series. The atomic states were obtained by diagonalizing the Dirac-Coulomb Hamiltonian matrix in the basis of *jj*-coupled antisymmetric configuration state functions of the same total angular momentum, projection, and parity.

In each of the isoelectronic cases, simulation with FAC was run in two parts: the first part featuring the initial decay of the 3*d*-hole state into the intermediate states, and the second part featuring the subsequent Auger decay of those intermediate states into their final states. During the first part of the simulation the configuration $3d^94s^24p^6$ is used to describe the initial 3*d*-hole state. The intermediate states (final states of the first part) are described by a set of configurations: $4s^04p^6$, $4s^24p^4$, $4p^4(5s, 4/5/6d)^2$, $4p^44d\,kd$, $4s4p^4(5s, md)$, $4/5s\,np^5$, np^5md, $4s^2np^3(5s, md)$, $4s^24p^2\ell p(5s, md)$, $4s^24p\,\ell p^2(5s, md)$, $4/5s\,4p^4\ell p$, $4/5s\,4p\,\ell p^4$, $4p^4\ell p\,md$, $4p\,\ell p^4md$, $4/5s\,4p^3\ell p^2$, and $4p^3\ell p^2md$, in which $n = 4$, 5, 6, 7, and 8; $m = 4$, 5, 6, 7, 8, and 9; $\ell = 5$, 6, 7, and 8; and $k = 5$, 6, 7, 8, and 9 (total of 32 480 states). The simulation of the decay into the states consisting of these configurations was run separately for even- and odd-parity cases.

Simulation of the second Auger decay was performed to obtain theoretical estimates for the lifetimes of the intermediate states, namely, the final states in the first step of the decay process. The final states (of the second step of the decay process) consist of configurations $4s^24p^3$, $4s^24p^2(5s, 4/5d)$, $4s^24p(5s^2, 4/5d^2, 4d5d)$, $4s\,4p^4$, $4s\,4p^3(5s, 4/5d)$, $4s\,4p^2(5s^2, 4/5d^2, 4d5d)$, $4p^5$, $4p^4(5s, 4/5d)$, and $4p^3(5s^2, 4/5d^2, 4s5d)$ (total of 1965 states). The calculated lifetimes contribute to the width of the peaks observed in the Auger spectrum seen in Fig. 2(d).

In order to get a more comprehensive understanding of the Auger processes at hand, they were also simulated with GRASP2K together with the RATIP suite [31,32]. Because of the limitations imposed by GRASP2K and to achieve convergence, a more limited configuration space was used. The initial 3*d*-hole state was described by $3d^94s^24p^6$, and the intermediate states consisted of configurations $4p^6$, $4s^24p^4$, $4s^24p^2(4d^2, 5s^2, 4d5d)$, $4s4p^5$, $4s4p^4(5s, 4/5/6d)$, and $4s^24p^3(5s, 4/5/6d)$ (total of 668 states). The states of the final step were described by configurations $4s^24p^3$, $4s^24p^2(5s, 4/5/6d)$, $4s4p^4$, $4s4p^34d$, $4s4p^24d^2$, and $4p^5$ (total of 390 states).

IV. DISCUSSION

We present here the decay of the $3d_{5/2}$ hole only, as the two $3d_j$ holes behave in a similar way. For the Kr and Rb cases this selection is enabled by using the multielectron coincidence technique, which provides a direct way to isolate Auger spectra from different initial ionic states.

The Auger spectra of the decay of the $3d_{5/2}$ hole in the isoelectronic series of atomic Br, Kr^+, and Rb^{2+} resemble each other, but interestingly also notable differences are observed. We show that the evolution of various equivalent line groups and the total intensity distribution within the series can be followed as a function of the atomic number *Z*. All the intermediate and final atomic states in the series are very sensitive to configuration mixing in the MCDF scheme, which

is the reason for some of the discrepancies in labeling in contrast with some earlier studies [8,16] as well as within the series regarding the leading configuration.

The $3d_{5/2}$ Auger spectrum in Br is the one we investigated experimentally in finer detail. Therefore, its assignment is discussed first, comparing it with the earlier work on the isoelectronic Kr^+ counterpart [8,16]. We then describe the trends observable in the isoelectronic series of Br, Kr^+, and Rb^{2+}.

A. Auger decay of the $3d_{5/2}$ hole in Br

The $j = 5/2$ component of the high-resolution Br $M_{4,5}NN$ Auger spectrum collected with the hemispherical electron energy analyzer (MBS-A1) at BL6U is presented in Fig. 2(b). It is compared with the lower-resolution spectrum obtained with the magnetic bottle spectrometer in Fig. 2(c). Comparison with the equivalent Auger spectra of the isoelectronic Kr^+ and Rb^{2+} in Fig. 3, and reference to the energy levels in Fig. 4, allows one to recognize the main features of the experimental Br Auger electron spectrum.

Starting from the higher kinetic energy side in Fig. 3, between 53 and 49 eV is a feature arising from decays to Br^+ $4s^24p^4$ levels, between 41 and 38 eV is a feature corresponding to $4s4p^5$ final states, and at 26.6 eV is a line corresponding to $4s^04p^6$ decay. In the following these configurations are labeled as **e**, **d** and **a**, respectively.

In addition to the main groups, the spectrum consists of many lines that are due to electron correlation (i.e., final-state configuration mixing). The calculations shown in Fig. 2(d) give their assignments. The first remark is the strong configuration mixing that is necessary to reproduce the spectrum. The strength of mixing is measured by using the squares of mixing coefficients and is considered strong if multiple configurations of the same J and parity contribute to the atomic state in near equal amounts. The calculations show that the Auger line observed at 38.42 eV in Fig. 2(b), which could be interpreted as the $4s4p^5\ ^1P$ state, is better described by the $4s^24p^34d$ ($\mathbf{c_1}$) configuration. In a similar way, the Auger line observed at 26.58 eV in Fig. 2(b) is characterized by strong mixing between $4s4p^44d$ ($\mathbf{b_2}$) and $4s^04p^6$ (**a**) configurations. This is in contrast with Nahon *et al.* [21] where the line was assigned as a pure $4s^04p^6$ state. The other configurations that are essential to reproduce the experimental Auger spectrum are $\mathbf{b_1}$: $4s4p^4(5s, 6/7/9d)$ and $\mathbf{c_{2x}}$: $4s^24p^3(5s, nd)$.

The Auger lines in the kinetic energy range from 28 to 38 eV present a structure in Br richer than that of its Kr^+ counterpart, where a peak dominates ($\mathbf{c_{2\,5d}}$) and is described by a $4s^24p^35d$ configuration. Theoretical inspection reveals that the lines in Br can be assigned to $\mathbf{c_{2x}}$ configurations $4s^24p^3n\ell$ in which $n\ell$ is the $5s$, $5d$, $6d$, $7d$, $8d$, or $9d$ orbital (in the order of decreasing kinetic energy) in the dominant configuration. On the lower-energy side of $\mathbf{c_{2x}}$, at about 25 eV kinetic energy, two line groups, **a**($\mathbf{b_2}$) and $\mathbf{b_1}$, with clear equivalents in the Kr^+ decay spectra (see Fig. 3 and Refs. [8,16]) are seen. The line group $\mathbf{c_1}$ in the calculated spectrum is not unambiguously identifiable from the measurement but has an equivalent in the Kr^+ spectrum. Based on the simulations the lines in the case of Br feature considerable $4s^04p^6$- $4s4p^4nd$ mixing all the way to $4s4p^49d$. The corresponding lines in

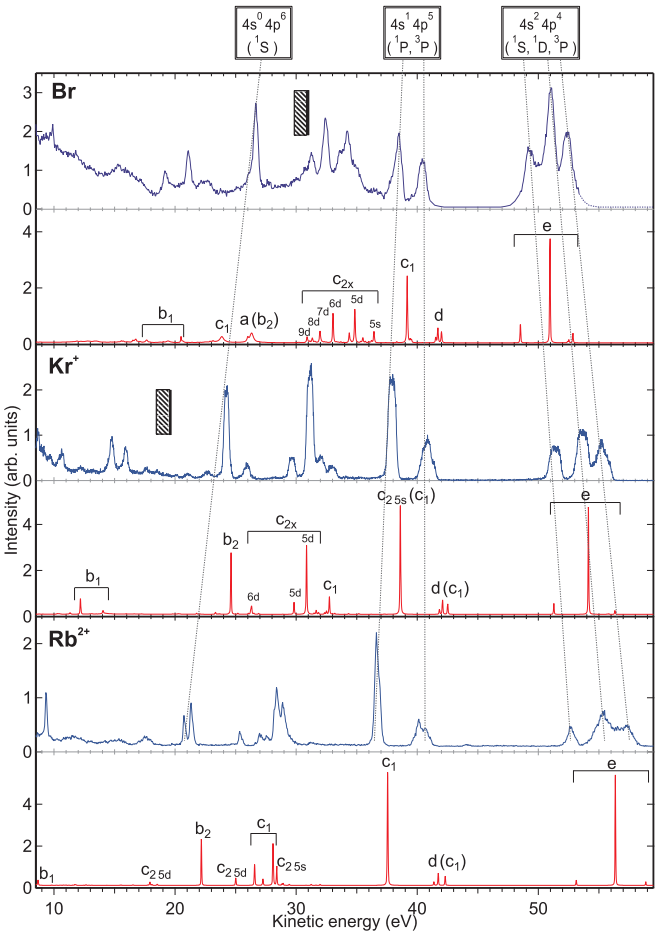

FIG. 3. Measured and simulated Auger spectra resulting from the decay of the $3d_{5/2}$ hole of the isoelectronic $3d^94s^24p^6$ states in the Br, Kr^+, and Rb^{2+} series. In each emboldened frame the upper panel (blue) depicts the experimental spectrum whereas the lower one (red) shows the results of the theoretical simulation (FAC) with the contribution of the subsequent Auger decay to the width added. Experimental intensities are the measured count numbers divided by 1000. Vertical lines with hatched areas in the Br and Kr^+ experimental spectra indicate the upper kinetic energy for the double-Auger path. Labels to assign the dominant configurations in the simulations are explained in the legend of Fig. 2.

Kr^+ feature a much weaker mixing. The strong mixing in Br can be attributed to the lower effective nuclear charge the electrons of Br experience when compared to Kr^+, which brings the $4s4p^4nd$ levels closer to the $4s^04p^6$ level and each other, which in turn increases configuration mixing. At around 20 eV kinetic energy an increasing background with few barely distinguishable features can be seen. This kind of increasing background at low kinetic energies is inherent to magnetic bottle data and is associated with secondary electrons emitted from surfaces. Our calculations, however, predict an intense line labeled as peak **a**, at around 10 eV in Fig. 2(d). The peak is clearly visible in the lifted dotted line representing the calculated spectrum without including the contribution of final-state broadening to the widths. The observation can be understood by considering the double-Auger decay of the $3d_{5/2}$ hole, as discussed in the following subsection. The sharp

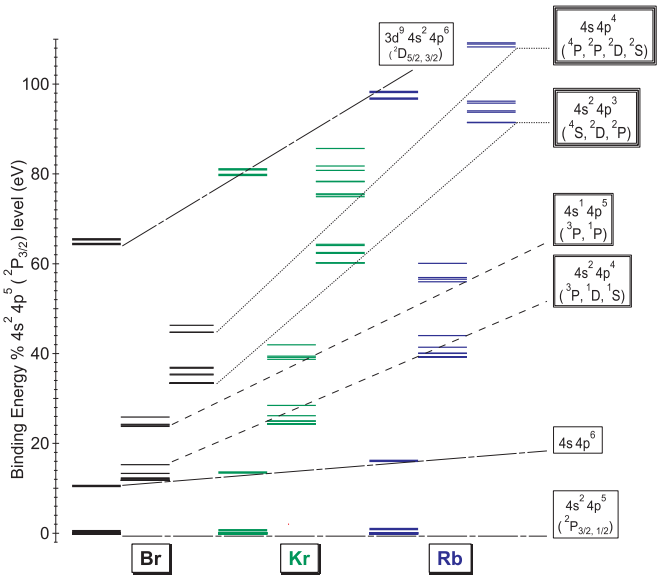

FIG. 4. Energy diagram showing states of interest in the Br, Kr^+, and Rb^{2+} series. For all species, the column on the left reports the energy levels of the $3d^{-1}4s^24p^6$ states, the middle one shows selected atomic states populated in single-Auger decay, and the one on the right gives states formed in double-Auger decay. All levels are referenced relative to the $3d^{10}4s^24p^5$ ($^2P_{3/2}$) ground state. The $3d^{-1}$ levels are obtained for Br from Ref. [19], for Kr^+ from Ref. [33], and for Rb^{2+} from the Ph.D. thesis of Khalal [18]. The other levels are from the NIST tables [34].

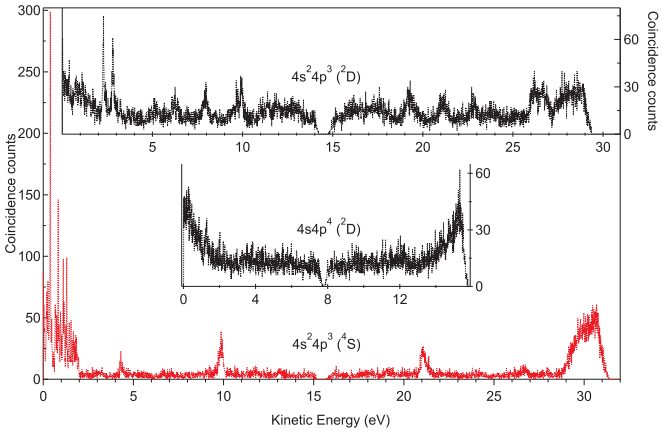

FIG. 5. Energy sharing between the two Auger electrons emitted in the double-Auger decay of the Br $3d_{5/2}$ hole and populating respectively the Br^{2+} $4s^24p^3$ (^2D), $4s^24p^3$ (^4S), or $4s4p^4$ (^2D) final states. The spectra are obtained from the intensities along the diagonal lines in Fig. 2(c) and the bin step for the three data curves is 10 meV.

peaks observed below 10 eV in the measured spectra in Fig. 2 are not reproduced in the calculated spectrum, because they correspond to second-step Auger electrons leading to the formation of Br^{2+} and are thus not included in the simulation of the first step.

B. Double-Auger decay of the $3d_{5/2}$ hole in Br

When comparing the double-Auger decay along the studied isoelectronic series, the first observation is that the kinetic energy of electrons involved increases with decreasing nuclear charge (up to 31 eV in Br, against 19.6 eV for Kr^+ and 5.3 eV for Rb^{2+}). The highest possible value can be deduced from the energy levels in Fig. 4 and is also indicated in Fig. 3 as striped vertical bars. Our coincidence experiments give an estimate of $38 \pm 5\%$ for the probability of the $3d_{5/2}$ hole to decay by emission of two Auger electrons in Br compared to a value of $28.4 \pm 1\%$ in Kr^+ [8]. This larger double-Auger probability is mainly explained by the fact that in the case of Br the intense Auger peak at 26.58 eV arising from Auger decay to the $4s^04p^6$ state lies in the double-Auger continuum, which allows it to decay further. As explained previously, our calculation shown in Fig. 2(d) finds the $4s^04p^6$ state to be strongly mixed with $4s4p^44d$ ($J = 0$) states. However, including the further decay of this state, shown as a solid line in Fig. 2(d), provides an overestimated width in comparison to the experimental observation.

The Br^{2+} states populated in the double-Auger decay of the $3d_{5/2}$ hole are displayed in Fig. 1(d). This spectrum is obtained by integrating along the constant excess energy in the two-dimensional spectrum shown in Fig. 1(c), as explained in the experimental part. One observes that this double-Auger decay populates mainly the $4s^24p^3$ (^4S, ^2D, ^2P) and $4s4p^4$ (^2D) Br^{2+} states. The intensity distribution along these lines is represented in Fig. 5 for three selected states. It gives an indication of the mechanisms of the double-Auger decay into these states. One observes peaks associated with cascade double-Auger decay and continuous intensity associated with direct double-Auger decay. This direct double-Auger path is observed as a u-shaped intensity of ~10–20 coincidence counts in Fig. 5. Interestingly this direct double-Auger decay populates the $4s^24p^3$ (^2D) and $4s4p^4$ (^2D) Br^{2+} states, but not the $4s^24p^3$ (^4S) one, which is essentially populated by cascade decays. The sharp peaks below 2 eV for the formation of this $4s^24p^3$ (^4S) Br^{2+} ground state indicate that the cascade decays involve mainly $4s^24p^3$ (^2D) $n\ell$ Br^+ intermediate states, which converge to the $4s^24p^3$ (^2D) Br^{2+} state. Note the continuity in intensity between the population of the high $4s^24p^3$ (^2D) $n\ell$ Br^+ Rydberg states and that of the $[4s^24p^3$ (^2D) $Br^{2+} + e^-]$ continuum. In other words, we observe a continuity between the direct double-Auger decay to the $4s^24p^3$ (^2D) Br^{2+} state and the cascade double-Auger decay through the associated $4s^24p^3$ (^2D) $n\ell$ Br^+ Rydberg states.

Other cascade double-Auger paths are observed in Figs. 1 and 5 and associated with Br^+ intermediate states. The calculations (dotted lines) in Fig. 2(d) identify several such states of $\mathbf{c_1}$ or $\mathbf{b_1}$ configuration (Auger lines respectively at 24 eV or between 15 and 20 eV). An intense Br^+ intermediate state of configuration **a** is also predicted to cause the Auger peak at 10 eV. The inclusion of its further cascade decay to the $4s4p^4$ (^2D) Br^{2+} state smears out the peak to a continuumlike structure. The calculated lifetime broadening of the line turned out to be very sensitive to the selected basis set, in a way that inclusion of a certain configuration mixing expanded the width to over 100 eV, which is clearly incorrect. The most reliable value, in terms of reproducibility with a varying set of configurations, we obtained is 12 eV, which corresponds to lifetime of about 30 as, but it is probably still somewhat

overestimated. The line is, however, an interesting demonstration of the power of very large final-state lifetime broadening to hide Auger electron lines when relying on conventional one-electron detection.

C. Comparison of the Auger decay of the $3d_{5/2}$ hole within the isoelectronic Br, Kr^+, and Rb^{2+} series

The experimental magnetic bottle time-of-flight measured Auger electron spectra resulting from the decay of the $3d^9_{5/2}4s^24p^6$ state in Br, Kr^+, and Rb^{2+} are presented as solid lines (blue) in the upper panels of their respective frames in Fig. 3. The lower panel of each frame shows the corresponding spectra (in red) simulated with FAC. The labeling scheme follows the one described for Br in Fig. 2.

The M_5NN Auger decay spectra of all three atoms in the isoelectronic series resemble each other to such a degree that it is possible to visually identify the corresponding line groups in the kinetic energy range from approximately 10 to 60 eV. We observe certain trends in Fig. 3 when moving from Br to Rb^{2+}. One such trend is the structure of the spectrum being richest in the case of Br and becoming simpler with Kr^+ and Rb^{2+}. The line group $\mathbf{c_1}/\mathbf{c_{2x}}$, which in Br spectrum can be found between 30 and 37 eV, lies at lower kinetic energies between 26 and 32 eV in the case of Kr^+ and between 25 and 30 eV in Rb^{2+}. According to our calculations the mixing between $4s4p^5$- $4s^24p^3nd$ configurations, where $n = 5, \ldots, 9$, decreases with increasing nuclear charge. This contribution gives the group its complex structure in the Br case. On the lower kinetic energy side of this group we see groups labeled $\mathbf{a}(\mathbf{b_2})/\mathbf{b_2}$, $\mathbf{c_1}/\mathbf{c_{2\,5d}}$ (absent in Kr^+), and $\mathbf{b_1}$ in the order of descending kinetic energy. The most intense peak in the $\mathbf{b_2}$ group at around 21 eV in the measured Rb^{2+} spectrum seems to be split in two, a feature not reproduced in our spectrum simulated with FAC. The discrepancy is discussed in the next subsection.

We can also see from Fig. 3 that except for line groups highest in kinetic energy **e** ($4s^24p^4$) and $\mathbf{d}(\mathbf{c_1})$ ($4s4p^5$), all the groups move towards lower kinetic energies as the atomic number increases within the isoelectronic series. Group **e** moves towards higher energy and the location of $\mathbf{d}(\mathbf{c_1})$ seems to stay relatively constant. Kinetic energies of Auger electrons represent differences in total energies between the initial and various final states of the first step of the decay. A selection of such states with respect to the $4s^24p^5\ {}^2P_{3/2}$ state is presented as an energy level diagram in Fig. 4. By looking at the diagram one can get an idea of how the energy levels behave as a function of Z. From the aforementioned trends within the isoelectronic series in Fig. 3 one can see that as Z increases the states characterized by the configuration $4s^24p^4$ (group **e** in Fig. 3) move further away (downwards in Fig. 4) from the the initial $3d^{-1}$ states, whereas the energy differences between the initial and the $4s4p^5$ states remains almost constant. The states dominated by the other configurations such as $4s^04p^6$, $4s4p^4(nd/5s)$, and $4s^24p^3(nd/5s)$ (labels **a**, $\mathbf{b_1}/\mathbf{b_2}$, and $\mathbf{c_1}/\mathbf{c_{2x}}$ in Fig. 3, respectively) move closer to the initial hole state as Z increases.

The reason for such opposite behavior of different intermediate states relative to the $3d^{-1}4s^24^6$ state lies in how the states are affected by an increase in the effective nuclear charge experienced by the electrons of interest when moving from Br to Rb^{2+}. The atomic states that shift towards lower energies or stay approximately the same relative to the initial $3d$-hole state as the atomic number Z increases are characterized by configurations $4s^24p^4$ (**e**) and $4s4p^5$ (**d**), respectively. The states in which the leading configuration is $4s^04p^6$ (**a**) or has $nd/5s$ ($n = 4, \ldots, 9$) orbital singly occupied move closer to the $3d$-hole state in energy (upwards in Fig. 4). From this one can see that the increasing effective nuclear charge has a stronger binding effect on the energies of states of $4s^24p^4$ and $4s4p^5$ configurations than on other states. The electrons in s subshells are in general more sensitive than those on other subshells to the changes in the nuclear charge. It should be noted that the general trends of the energies of the line groups can be described even in the single-configuration scheme, which rules out the influence of configuration interaction on the observed behavior.

D. Complementary information on Auger decay of the $3d_{5/2}$ hole in Kr^+ and Rb^{2+}

The present identifications of the peaks in the Kr^+ spectrum are in agreement with studies [8,16], though it is noted that the main contributing configurations are not always identical. This discrepancy can be attributed to the atomic states in this energy region being sensitive to configuration interaction. The effect can be easily observed in Fig. 3 at around 40 eV with the $\mathbf{d}/\mathbf{c}_1$ line group, which has a simple structure and can be reproduced in computations even with a single-configuration calculation including the $4s4p^5$ (**d**) configuration. In the multiconfiguration scheme, $4s4p^5$, however, is not the leading configuration for all the lines in the group throughout the isoelectronic series as it readily mixes with the $4s^24p^34d$ configuration. The overall shape and the intensity distribution are, however, similar between single-configuration and multiconfiguration calculations.

The seemingly split peak in the Rb^{2+} Auger spectrum at about 21 eV kinetic energy in the measured spectrum in Fig. 3 is not reproduced by the FAC calculations. To study this feature and investigate the sensitivity of calculations to the selected atomic code, Fig. 6 provides comparison between Rb^{2+} M_5NN Auger spectra obtained using GRASP2K and FAC.

As can be seen, the GRASP2K calculation presented in the middle panel of Fig. 6 reproduces the double-peak structure at about 24 eV kinetic energy. According to the analysis based on the GRASP2K calculation the structure is not a split peak, but instead two lines originating from decays into states of opposite parity. Based on the FAC calculation, the line at lower kinetic energy has been identified to belong to the $4s4p^44d$ ($\mathbf{b_2}$) group earlier in this section. The line can be found throughout the isoelectronic series as can be seen in Fig. 3. The GRASP2K simulation, however, suggests that the leading configuration of the state is $4s^04p^6$ (**a**) with $4s4p^44d$ ($\mathbf{b_2}$) as the second-largest contributor. This difference between the two calculations further demonstrates the sensitivity of simulations of these atomic states to the effects of configuration interaction and small numerical differences.

The peak on the higher kinetic energy side seems to be absent in the FAC simulation, but based on calculations with GRASP2K, can be assigned to the $4s^24p^34d$ ($\mathbf{c_1}$) group. This

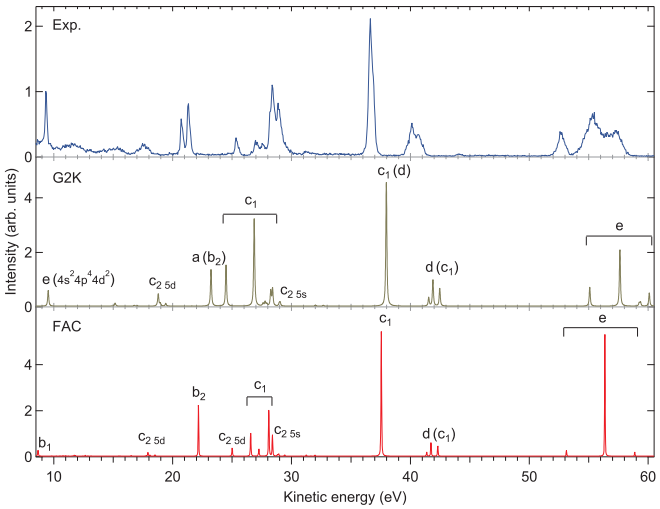

FIG. 6. Comparison of the measured Auger spectrum resulting from the decay of the Rb^{2+} $3d_{5/2}^{-1}$ state with the spectrum simulated using GRASP2K (brown) and FAC (red) presented in kinetic energy. Experimental intensities are the measured count numbers divided by 1000. Labels to assign the dominant configurations in the simulations are explained in the legend of Fig. 2.

makes the peak a part of the line group stretching from 24 to 29 eV and defined by $\mathbf{c_1}/\mathbf{c_{2x}}$ in the middle panel of Fig. 6; thus in the FAC calculation the corresponding line is $\mathbf{c_{2\,5d}}$ at 25 eV. This interpretation means that these two lines happen to lie at almost the same energy, appearing as something which at a glance looks like a split peak. The smaller configuration space used in the GRASP2K calculations seems to be able to reproduce the decay spectrum in the case of Rb^{2+} better than FAC. On the other hand, for Br and Kr^+, the large set used in FAC yields better results.

V. CONCLUSIONS

The Auger decay following the $3d_{5/2}$-hole state in the electron configuration $3d^{-1}4s^24p^6$ was studied using synchrotron radiation and recorded with a magnetic bottle time-of-flight setup for the isoelectronic series of Br, Kr^+, and Rb^{2+}. The $3d_{5/2}$-hole decay spectrum in Br was also recorded with a high-resolution hemispherical energy analyzer. Interpretation of the results was done with the aid of MCDF calculations and, in contrast with earlier studies, complemented by the study of the evolution of experimental and theoretical line energies along the isoelectronic series. A good agreement, albeit with some differences in the predicted intensities, between the measurements and theoretical predictions was reached, which enabled us to identify the lines visible in the Br Auger decay spectrum and interpret the corresponding coincidence map as well as discover trends in the spectral features within the studied isoelectronic series.

The $3d_{5/2}$ double-Auger decay is found to be more probable in Br than in the other systems, based on energy considerations from Fig. 4 and on our coincidence measurements. An increased contribution of electron configurations, in which the nd $(n = 4, \ldots, 9)$ subshell is singly occupied, was observed in Br. The strength of the configuration interaction was found to be inversely proportional to the atomic number Z within the isoelectronic series. This and the observed evolution of the energies of different corresponding states within the series are attributed to the increased effective nuclear charge experienced by the electrons of interest as Z increases.

ACKNOWLEDGMENTS

We are grateful to R. Püttner for his help during the measurements and to the BESSY and UVSOR staff for the stable operation of the synchrotrons during these measurements. This work has been financially supported in part by the European Community, Research Infrastructure Action, under the FP6 "Structuring European Research Area" Programme (Contract No. R II 3-CT-2004-506008), and by the Research Council for Natural Sciences and Engineering of the Academy of Finland. P.L. acknowledges the support of the Institute of Molecular Science and J.K. acknowledges EXACTUS-DP (Doctoral Program in Exact Sciences), The Magnus Ehrnrooth Foundation, and the Vilho, Yrjö and Kalle Väisälä Fund.

[1] L. Meitner, Z. Phys. **9**, 145 (1922).
[2] P. Auger, J. Phys. Radium **6**, 205 (1925).
[3] T. A. Carlson and M. O. Krause, Phys. Rev. Lett. **14**, 390 (1965).
[4] T. A. Carlson and M. O. Krause, Phys. Rev. Lett. **17**, 1079 (1966).
[5] P. Lablanquie, S. Sheinerman, F. Penent, R. I. Hall, M. Ahmad, Y. Hikosaka, and K. Ito, Phys. Rev. Lett. **87**, 053001 (2001).
[6] J. Viefhaus, S. Cvejanović, B. Langer, T. Lischke, G. Prümper, D. Rolles, A. V. Golovin, A. N. Grum-Grzhimailo, N. M. Kabachnik, and U. Becker, Phys. Rev. Lett. **92**, 083001 (2004).
[7] F. Penent, J. Palaudoux, P. Lablanquie, L. Andric, R. Feifel, and J. H. D. Eland, Phys. Rev. Lett. **95**, 083002 (2005).
[8] J. Palaudoux, P. Lablanquie, L. Andric, K. Ito, E. Shigemasa, J. H. D. Eland, V. Jonauskas, S. Kučas, R. Karazija, and F. Penent, Phys. Rev. A **82**, 043419 (2010).
[9] A. G. Kochur, V. L. Sukhorukov, A. J. Dudenko, and P. V. Demekhin, J. Phys. B: At., Mol. Opt. Phys. **28**, 387 (1995).
[10] J. Zeng, P. Liu, W. Xiang, and J. Yuan, Phys. Rev. A **87**, 033419 (2013).
[11] A. Müller, A. Borovik, Jr., T. Buhr, J. Hellhund, K. Holste, A. L. D. Kilcoyne, S. Klumpp, M. Martins, S. Ricz, J. Viefhaus, and S. Schippers, Phys. Rev. Lett. **114**, 013002 (2015).
[12] P. Lablanquie, M. A. Khalal, L. Andric, J. Palaudoux, F. Penent, J.-M. Bizau, D. Cubaynes, K. Jänkälä, Y. Hikosaka, K. Ito, K. Bučar, and M. Žitnik, J. Electron Spectrosc. Relat. Phenom. **220**, 125 (2017).
[13] W. Mehlhorn, Z. Phys. **187**, 21 (1965).
[14] H. Aksela, S. Aksela, and H. Pulkkinen, Phys. Rev. A **30**, 2456 (1984).

[15] J. Jauhiainen, H. Aksela, S. Aksela, A. Kivimäki, O.-P. Sairanen, E. Nõmmiste, and J. Végh, J. Phys. B **28**, 3831 (1995).
[16] L. Partanen, M. Huttula, H. Aksela, and S. Aksela, J. Phys. B **40**, 3795 (2007).
[17] V. Jonauskas, R. Karazija, and S. Kučas, J. Phys. B **41**, 215005 (2008).
[18] M. A. Khalal, Ph.D. thesis, UPMC University of Paris 6, 2018, and linking to, https://hal.archives-ouvertes.fr/tel-02434742.
[19] M. Mazzoni and M. Pettini, Phys. Lett. A **85**, 331 (1981).
[20] A. Cummings and G. O'Sullivan, Phys. Rev. A **54**, 323 (1996).
[21] L. Nahon, P. Morin, and F. Combet-Farnoux, Phys. Scr. **1992**, 104 (1992).
[22] P. Morin and I. Nenner, Phys. Rev. Lett. **56**, 1913 (1986).
[23] P. Lablanquie, H. Iwayama, F. Penent, K. Soejima, and E. Shigemasa, J. Electron Spectrosc. Relat. Phenom. **195**, 96 (2014).
[24] X.-J. Liu, Q. Miao, F. Gel'mukhanov, M. Patanen, O. Travnikova, C. Nicolas, H. Ågren, K. Ueda, and C. Miron, Nat. Photonics **9**, 120 (2014).
[25] S.-M. Huttula, P. Lablanquie, L. Andric, J. Palaudoux, M. Huttula, S. Sheinerman, E. Shigemasa, Y. Hikosaka, K. Ito, and F. Penent, Phys. Rev. Lett. **110**, 113002 (2013).
[26] M. A. Khalal, P. Lablanquie, L. Andric, J. Palaudoux, F. Penent, K. Bučar, M. Žitnik, R. Püttner, K. Jänkälä, D. Cubaynes, S. Guilbaud, and J.-M. Bizau, Phys. Rev. A **96**, 013412 (2017).
[27] K. J. S. Sawhney, F. Senf, M. Scheer, F. Schäfers, J. Bahrdt, A. Gaupp, and W. Gudat, Nucl. Instrum. Methods Phys. Res., Sect. A **390**, 395 (1997).
[28] M. F. Gu, Can. J. Phys. **86**, 675 (2008).
[29] F. A. Parpia, C. Froese Fischer, and I. P. Grant, Comput. Phys. Commun. **94**, 249 (1996).
[30] P. Jönsson, X. He, C. Froese Fischer, and I. P. Grant, Comput. Phys. Commun. **177**, 597 (2007).
[31] S. Fritzsche, J. Electron Spectrosc. Relat. Phenom. **114-116**, 1155 (2001).
[32] S. Fritzsche, Comput. Phys. Commun. **187**, 1525 (2012).
[33] G. C. King, M. Tronc, F. H. Read, and R. C. Bradford, J. Phys. B: At. Mol. Phys. **10**, 2479 (1977).
[34] A. Kramida, Y. Ralchenko, J. Reader, and NIST ASD Team (2019), NIST Atomic Spectra Database (version 5.7.1), National Institute of Standards and Technology, Gaithersburg, MD, US, retrieved from https://www.nist.gov/pml/atomic-spectra-database on February 18, 2021.